Regulation of peripheral T cell activation by calreticulin

Simona Porcellini,[1] Elisabetta Traggiai,[1] Ursula Schenk,[1] Denise Ferrera,[1] Michela Matteoli,[2] Antonio Lanzavecchia,[1] Marek Michalak,[3] and Fabio Grassi[1]

[1]Institute for Research in Biomedicine, CH-6500 Bellinzona, Switzerland
[2]Department of Medical Pharmacology, CNR Institute of Neuroscience, Cellular and Molecular Pharmacology, Center of Excellence for Neurodegenerative Diseases, 20129 Milano, Italy
[3]Department of Biochemistry, University of Alberta, Edmonton, Alberta T6G 2H7, Canada

Regulated expression of positive and negative regulatory factors controls the extent and duration of T cell adaptive immune response preserving the organism's integrity. Calreticulin (CRT) is a major Ca^{2+} buffering chaperone in the lumen of the endoplasmic reticulum. Here we investigated the impact of CRT deficiency on T cell function in immunodeficient mice reconstituted with fetal liver *crt*$^{-/-}$ hemopoietic progenitors. These chimeric mice displayed severe immunopathological traits, which correlated with a lower threshold of T cell receptor (TCR) activation and exaggerated peripheral T cell response to antigen with enhanced secretion of inflammatory cytokines. In *crt*$^{-/-}$ T cells TCR stimulation induced pulsatile cytosolic elevations of Ca^{2+} concentration and protracted accumulation of nuclear factor of activated T cells in the nucleus as well as sustained activation of the mitogen-activated protein kinase pathways. These observations support the hypothesis that CRT-dependent shaping of Ca^{2+} signaling critically contributes to the modulation of the T cell adaptive immune response.

CORRESPONDENCE
Fabio Grassi:
fabio.grassi@irb.unisi.ch

Abbreviations used: $[Ca^{2+}]_i$, intracellular free Ca^{2+}; CRT, calreticulin; DKO, double knockout; DP, double positive; FLP, fetal liver hemopoietic progenitor; MAPK, mitogen-activated protein kinase; OVAp, OVA peptide; SERCA, sarco-endoplasmic reticulum calcium transport ATPase; SP, single positive; T reg, T regulatory.

T cell interaction with antigen-presenting cells in antimicrobial immune response stimulates a cascade of TCR-driven signal transduction events, which eventually results in clonal expansion, activation of effector functions, and generation of memory. Positive and negative regulatory feedback loops influence stimulation threshold as well as propagation and persistence of signals in the various phases of the response (1). The correct regulation of all elements involved in the T cell response to antigen ensures appropriate T cell expansion, differentiation, and homeostasis. Indeed, defects in negative regulatory molecules, such as phosphatases (2, 3), E3 ubiquitin ligases (4, 5), cell surface receptors (6), and transcription factors (7, 8), contribute to the development of immunopathology. Defects in the induction of apoptosis were shown to affect the deletion of autoreactive cells in the thymus, resulting in autoimmune pathology in the periphery (9). Apoptosis is also critical in determining the contraction of the immune response to a given pathogen (10). The identification of elements that selectively influence the outcome of TCR stimulation at distinct phases of T cell development and differentiation is of great importance for understanding the functioning of the adaptive immune system.

A crucial signal for T cell response after agonist binding to the TCR is the elevation of intracellular free Ca^{2+} ($[Ca^{2+}]_i$), which is contributed by both release from intracellular stores and influx from extracellular space through Ca^{2+} release–activated Ca^{2+} channels in the plasma membrane (11). Moreover, different amplitudes and frequencies of $[Ca^{2+}]_i$ elevations in the lymphocyte were shown to differentially regulate activation of transcription factors crucially involved in the immune response (12, 13). Among these factors, NFAT is dephosphorylated and translocated to the nucleus upon activation of the phosphatase calcineurin by $[Ca^{2+}]_i$ increase (14). Members of the NFAT family were shown to participate both as positive as well as negative regulators of the T cell response to antigen (15).

Calreticulin (CRT) is a Ca^{2+} binding chaperone protein predominantly localized

The online version of this article contains supplemental material.

in the ER where it assists the folding of glycoproteins (16). The protein may be divided into three structural and functional domains: the NH_2-terminal N-domain, which is extremely conserved and likely participates in the folding of specific substrates and, together with the extended proline-rich P-domain, has a lectin-like chaperone activity. The acidic COOH-terminal C-domain with low affinity, high avidity for Ca^{2+} contributes to the Ca^{2+} storage capacity of the ER (17). The amount of CRT-bound Ca^{2+} in the ER may dramatically influence the cell fate; e.g., overexpression of CRT leads to increased susceptibility to apoptotic stimuli (18), whereas CRT-deficient cells are more resistant to apoptosis (19). CRT deficiency in mice is embryonically lethal because of altered cardiac development, and the majority of $crt^{-/-}$ embryos die at day 12–13 of gestation (20). In embryonic $crt^{-/-}$ cardiomyocyte, defective Ca^{2+} release from the ER upon agonist stimulation results in defective calcineurin-dependent activation of myocyte enhancer factor 2C and contributes significantly to embryonic lethality (21). Indeed, transgenic expression of a constitutively active isoform of calcineurin in the hearth resumed myofibrillogenesis in $crt^{-/-}$ embryos (22).

To study the impact of CRT deficiency on lymphocyte function we generated fetal liver chimeric mice by reconstituting RAG-2/common γ chain double knockout (DKO) mice with fetal liver hemopoietic progenitors (FLPs) from $crt^{-/-}$ embryos. $Crt^{-/-}$ fetal liver chimeras displayed immunopathological traits that correlated with exaggerated responsiveness to TCR stimulation, increased cytokine production, reduced apoptosis, and altered regulation of signaling in peripheral T cells. These observations suggest that CRT plays a crucial role in regulating the effector phase of the adaptive immune response.

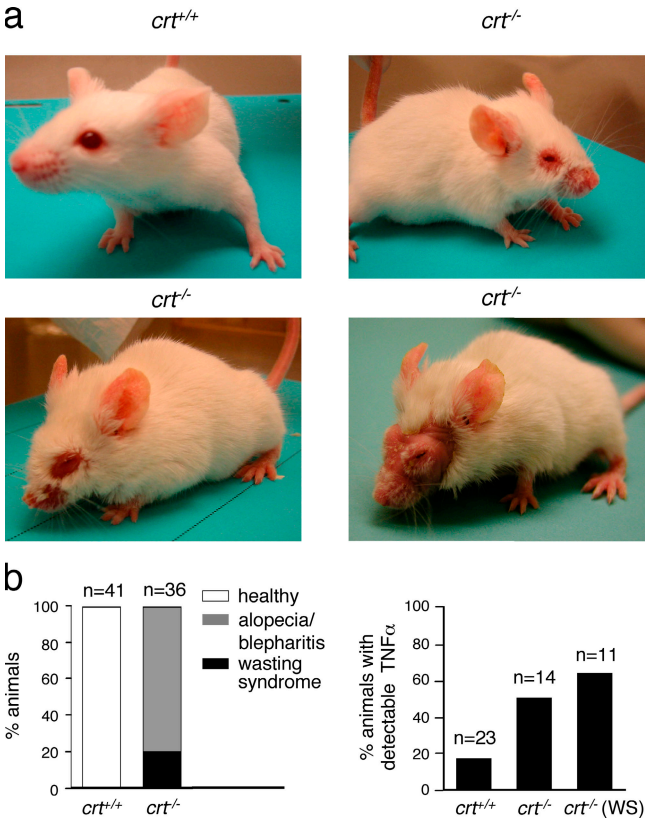

Figure 1. Phenotype of chimeric mice. (a) RAG/γ chain DKO mice reconstituted with $crt^{+/+}$ and $crt^{-/-}$ FLPs at weeks 12 ($crt^{+/+}$), 8 ($crt^{-/-}$, top right), 10 ($crt^{-/-}$, bottom left), and 12 ($crt^{-/-}$, bottom right) after reconstitution. (b) Relative distributions of chimeric mice with respect to phenotype (left) and detection of TNF-α in the serum (>2 pg/ml). WS, wasting syndrome.

RESULTS

Immunopathological phenotype of $crt^{-/-}$ fetal liver chimeras

RAG/γ chain DKO mice reconstituted with $crt^{-/-}$ FLPs display alopecia and blepharitis starting at week 7 after reconstitution (Fig. 1 a). Histological analysis of the skin revealed epidermis hyperplasia and an inflammatory infiltrate (not depicted). An inflammatory infiltrate was also evident in the peribronchial space of the lung, whereas the thymus, gut, kidney, liver, and pancreas were histologically unaltered. Antinuclear, anti–double-stranded DNA, and anti-cardiolipin antibodies were absent from the sera of both $crt^{+/+}$ ($n = 22$) and $crt^{-/-}$ ($n = 20$) chimeras (see Supplemental Materials and methods, available at http://www.jem.org/cgi/content/full/jem.20051519/DC1); however, IgG_1 and IgE serum levels were significantly increased in $crt^{-/-}$ chimeras ($crt^{+/+}$, $n = 26$: $IgG_1 = 1.5 \pm 0.7$ mg/ml, IgE $= 1.1 \pm 2.4$ μg/ml; $crt^{-/-}$, $n = 24$: $IgG_1 = 5.8 \pm 3.0$ mg/ml, $P < 0.0001$, IgE $= 10.5 \pm 14.5$ μg/ml, $P = 0.002$). The immunopathology and higher immunoglobulin levels in $crt^{-/-}$ chimeric mice were dependent on T cells because $crt^{-/-}/cd3\varepsilon^{-/-}$ DKO chimeras were healthy up to 20 wk after reconstitution and did not display significant differences with respect to $crt^{+/+}/cd3\varepsilon^{-/-}$ DKO chimeras in serum IgG_1 ($crt^{+/+} = 4.6 \pm 3.8$ μg/ml, $n = 4$; $crt^{-/-} = 3.4 \pm 2.9$ μg/ml, $n = 8$) and IgE, which were undetectable. 20% of $crt^{-/-}$ mice developed a wasting syndrome that correlated with a relative increase in the detection of TNF-α in the serum (Fig. 1 b). Indeed, overproduction of TNF-α has been shown to be involved in the pathogenesis of different disease states, and the expression of a TNF-α transgene in T cells determined the development of a wasting syndrome (23). Analysis of T cells from lymph nodes and spleen revealed an increase in the CD4/CD8 ratio in $crt^{-/-}$ chimeras (Fig. 2 a). Absolute numbers of CD4 cells in the spleen were not significantly increased ($crt^{+/+} = 11.0 \pm 5.8 \times 10^6$, $n = 35$; $crt^{-/-} = 10.8 \pm 5.8 \times 10^6$, $n = 39$). Both CD4 and CD8 subsets displayed increased percentages of activated cells, as determined by CD69 and CD25 expression (Fig. 2 b). In the CD4 subset, both $CD25^+69^+$ and $CD25^+69^-$ cells were significantly increased in $crt^{-/-}$ versus $crt^{+/+}$ chimeras ($CD25^+69^+$: $crt^{-/-}$, $15.5 \pm 5.3\%$, $n = 4$; $crt^{+/+}$, $4.8 \pm 1.1\%$, $n = 5$, $P = 0.003$; $CD25^+69^-$: $crt^{-/-}$, $12.3 \pm 2.1\%$, $n = 4$; $crt^{+/+}$, $7.4 \pm 1.4\%$, $n = 5$, $P = 0.004$). Intracellular staining for IL-2, IFN-γ, and TNF-α of freshly isolated peripheral T cells treated with brefeldin A, ionomycin, and PMA revealed increased percentages of cells producing these cytokines (Fig. 2 c).

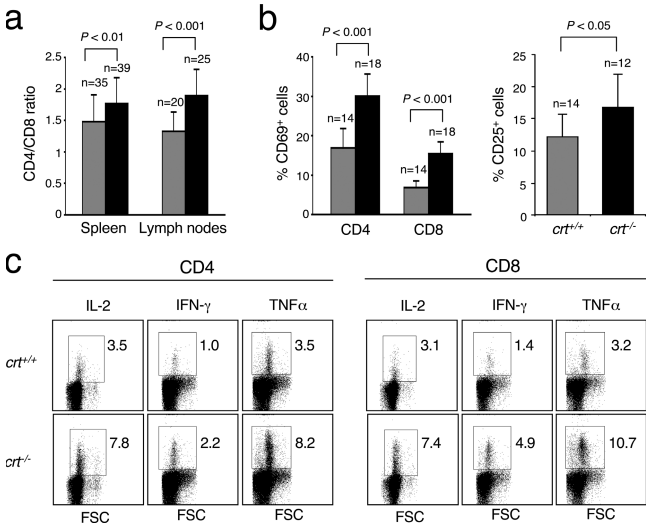

Figure 2. Increased CD4/CD8 ratio, augmented representations of activated T cells, and cytokine secretion by ex vivo *crt*$^{-/-}$ T cells. (a) CD4/CD8 ratios in the spleen and lymph nodes. (b) Relative representations of CD69$^+$ cells in CD4$^+$ and CD8$^+$ subsets (left) and CD25$^+$ cells in CD4$^+$ subset (right). Gray bars, *crt*$^{+/+}$ chimeras; black bars, *crt*$^{-/-}$ chimeras. (c) Ex vivo cytokine secretion of CD4$^+$ and CD8$^+$ T cells. Intracellular staining for the indicated cytokine was performed on freshly isolated lymph node cells treated with PMA, ionomycin, and brefeldin A (see Materials and methods). This experiment is representative of six different mice per group.

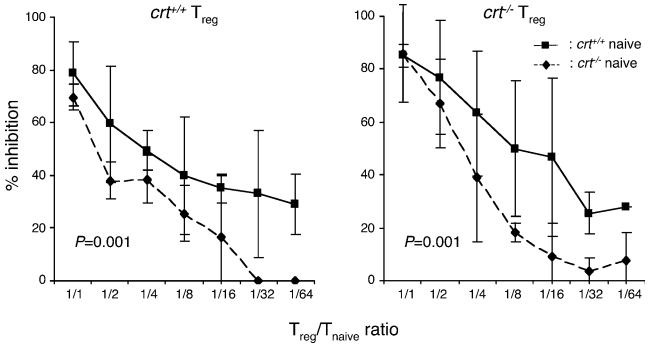

Figure 3. Efficient function of *crt*$^{-/-}$ T reg cells and decreased sensitivity of *crt*$^{-/-}$ naive T cells to T reg cell–mediated suppression. Inhibition of CD3ε mitogenic response of *crt*$^{+/+}$ (■) and *crt*$^{-/-}$ (◆) naive T cells by purified CD4$^+$CD25$^+$ cells from *crt*$^{+/+}$ (left) or *crt*$^{-/-}$ (right) chimeric mice. Values are means ± SD of three independent experiments.

Thymocyte development in *crt*$^{-/-}$ chimeric mice

Because pre-TCR (24) and αβTCR (25–27) signaling induce $[Ca^{2+}]_i$ elevations during thymocyte development, we tested whether CRT deficiency interfered with T cell differentiation in the thymus. Immature thymocyte subset representation did not reveal an altered pre-TCR signaling in *crt*$^{-/-}$ thymocyte (see Supplemental Results and Fig. S1, available at http://www.jem.org/cgi/content/full/jem.20051519/DC1). Next, we checked whether CRT deficiency affected positive selection of αβTCR$^+$ CD4$^+$8$^+$ double positive (DP) cells. Cell recoveries (*crt*$^{+/+}$: 45.8 ± 27.8 × 10^6, n = 40; *crt*$^{-/-}$: 42.9 ± 26.6 × 10^6, n = 30) and CD4/CD8 ratios (*crt*$^{+/+}$: 2.79 ± 0.65, n = 24; *crt*$^{-/-}$: 2.43 ± 0.97, n = 25) of thymi analyzed between weeks 6 and 20 after reconstitution were not significantly different. Thymocyte subset distribution with respect to CD4 and CD8 expression revealed a modest but statistically significant reduction of the DP compartment with relative increases of both CD4 and CD8 single positive (SP) cells (Fig. S1). DP cell contraction was most severe in the atrophic thymi obtained from animals affected by the wasting syndrome (not included in the statistical analysis) in which DP cells were undetectable. We imputed DP cell reduction in *crt*$^{-/-}$ chimeras to circulating proinflammatory cytokines affecting DP cell viability. Up-regulation of αβTCR and CD69 in DP cells as well as CD69 expression in CD4$^+$ and CD8$^+$ SP cells were all unaffected, suggesting that positive selection was occurring analogously in *crt*$^{-/-}$ as well as *crt*$^{+/+}$ thymocyte (Fig. S1). It was possible that a thymocyte expressing a given TCR responded differently to positively selecting signals in the absence of CRT. Then, H-2^b *crt*$^{-/+}$ mice were crossed with H-2^d mice transgenic for the I-A^d–restricted DO11.10 TCR specific for the OVA peptide (OVAp) 323–339 (28). The *crt*$^{-/+}$/DO11.10tg progeny was intercrossed and H-2$^{b/d}$ *crt*$^{-/-}$ as well as *crt*$^{+/+}$/DO11.10tg embryos were identified. Analysis of T cell development in fetal thymus organ culture with thymi from H-2$^{d/b}$ DO11.10tg *crt*$^{-/-}$ and *crt*$^{+/+}$ embryos did not reveal differences in CD69 expression in both DO11.10tg DP cells and DO11.10tg CD4$^+$ SP cells (Fig. S1), implying unaltered positive selection of DO11.10tg thymocytes in the absence of CRT. CRT deficiency decreases the sensitivity of a cell to apoptosis (19); thus, we checked whether this behavior was also common to thymocytes undergoing negative selection in the thymus. To assess thymocyte sensitivity to apoptosis we analyzed in vivo deletion by endogenous superantigens and in vitro induction of apoptosis in different assays (see Supplemental Results and Fig. S2, available at http://www.jem.org/cgi/content/full/jem.20051519/DC1). None of these experiments revealed a significant impairment of the clonal deletion process in *crt*$^{-/-}$ thymocytes. We concluded that CRT deficiency was not manifestly affecting either pre-TCR– or αβTCR-driven responses in the thymocyte.

Normal functional activity of T regulatory (T reg) cells from *crt*$^{-/-}$ chimeras, but reduced sensitivity of *crt*$^{-/-}$ T cells to T reg cell–mediated suppression

The CD4$^+$25$^+$ T reg cell subset exerts a crucial role in controlling anti-self immune responses (29) as well as the extent of T cell effector responses, thus inhibiting possible tissue damage resulting from antimicrobial immune responses (30). The abnormal activation of T cells in the periphery of *crt*$^{-/-}$ chimeras could be due to inefficient function of the T reg cell subset. CD4$^+$25$^+$ cells were purified from *crt*$^{-/-}$ as well as *crt*$^{+/+}$ chimeras and challenged for immunoregulatory competence in inhibition of the mitogenic response of naive T cells to CD3ε antibodies. The same efficiency in inhibiting the proliferative response of *crt*$^{+/+}$ naive T cells was detected for

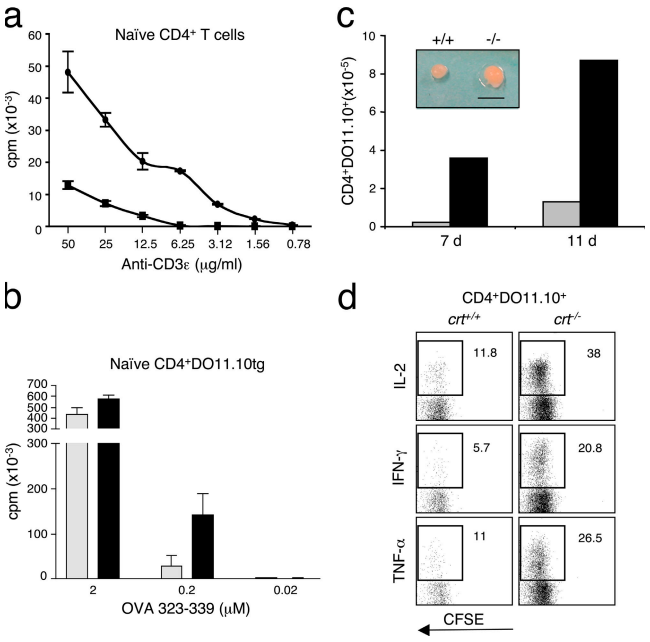

Figure 4. Enhanced in vitro and in vivo responsiveness of *crt*$^{-/-}$ naive T cells. (a) [^{3}H]thymidine incorporation in purified naive CD4$^+$ T cells stimulated with decreasing doses of plate-bound CD3ε mAb. ●, *crt*$^{-/-}$; ■, *crt*$^{+/+}$. cpm values (±SD) are from a single experiment representative of three. (b) DCs were loaded with the indicated concentrations of OVAp and used to stimulate purified naive CD4$^+$ cells from DO11.10tg *crt*$^{+/+}$ (gray bars) and *crt*$^{-/-}$ (black bars) chimeras. The displayed results are representative of four different experiments. Similar proportions of TCR transgenic cells were present in both *crt*$^{+/+}$ and *crt*$^{-/-}$ naive T cell suspensions in all experiments (from 75 to 90%). (c) CD4$^+$DO11.10tg H-2$^{d/b}$ *crt*$^{+/+}$ (gray bars) and *crt*$^{-/-}$ (black bars) cell recoveries from draining lymph nodes of adoptively transferred H-2$^{b/d}$ mice immunized with OVAp-loaded DCs into the footpad at days 7 and 11 from immunization. The inset shows two representative draining lymph nodes at day 11 from immunization. Bar, 0.5 cm. (d) Intracellular staining for the indicated cytokine versus CFSE dilution of electronically gated CD4$^+$DO11.10tg H-2$^{b/d}$ cells from the draining lymph nodes of adoptively transferred H-2$^{b/d}$ mice immunized with OVAp-loaded DCs at day 7 after immunization. This experiment was repeated three times with at least two animals/groups/time points with comparable results.

both *crt*$^{-/-}$ and *crt*$^{+/+}$ T reg cells, indicating that T reg cells were not intrinsically affected by CRT deficiency. However, the proliferation of *crt*$^{-/-}$ naive T cells was less efficiently inhibited by T reg cells purified from both *crt*$^{-/-}$ and *crt*$^{+/+}$ chimeras (Fig. 3), suggesting that *crt*$^{-/-}$ T cells were less susceptible to T reg cell–mediated suppression than *crt*$^{+/+}$ T cells.

In vitro– and in vivo–enhanced responsiveness of *crt*$^{-/-}$ naive T cells

To determine whether *crt*$^{-/-}$ T cells were more responsive to TCR triggering we purified CD4$^+$CD44$^-$CD25$^-$CD62L$^+$ naive T cells from chimeric mice. Both *crt*$^{+/+}$ and *crt*$^{-/-}$ naive T cells were stimulated with decreasing concentrations of immobilized CD3ε antibodies. *Crt*$^{-/-}$ naive T cells responded robustly to concentrations of CD3ε antibodies that were nonmitogenic for *crt*$^{+/+}$ cells (Fig. 4 a). To analyze the impact of CRT deficiency on the T cell response to antigen, H-2$^{b/d}$ *crt*$^{-/-}$ and *crt*$^{+/+}$/ DO11.10tg FLPs were used to reconstitute H-2^d RAG/γ chain DKO mice. Naive CD4$^+$DO11.10tg T cells from the lymph nodes and spleens of reconstituted mice were sorted and stimulated in vitro with I-A^d DCs loaded with different concentrations of OVAp. Fig. 4 b shows that whereas DCs pulsed with 2 μM OVAp generated comparable responses in *crt*$^{-/-}$ versus *crt*$^{+/+}$ cells, pulses with 0.2 μM OVAp generated robust proliferation of *crt*$^{-/-}$ but not *crt*$^{+/+}$ T cells. To analyze the response of DO11.10tg cells in vivo, splenocytes from reconstituted mice containing 10^6 CD4$^+$DO11.10tg T cells were labeled with CFSE and injected into H-2$^{b/d}$ mice. After 48 h mice were challenged with I-A^d DCs loaded with OVAp into the footpad. Inspection of the draining lymph nodes of mice adoptively transferred with *crt*$^{-/-}$ cells revealed more prominent swelling than those of mice transferred with *crt*$^{+/+}$ cells. Moreover, *crt*$^{-/-}$ DO11.10tg cells underwent more robust expansion and displayed increased cytokine secretion with respect to the *crt*$^{+/+}$ counterpart (Fig. 4, c and d). These data demonstrate that naive T cells from *crt*$^{-/-}$ chimeras undergo exaggerated responses upon antigen encounter.

Increased representation in vivo and hyperresponsiveness of *crt*$^{-/-}$ effector–memory T cells

Analysis of peripheral T cells for representation of effector–memory cells as determined by the CD44$^+$CD62L$^-$ phenotype revealed an increase of this subset in both CD4 and CD8 *crt*$^{-/-}$ T cell populations (Fig. 5 a). To test whether effector–memory T cells derived from *crt*$^{+/+}$ and *crt*$^{-/-}$ fetal liver chimeras might differ in their activation threshold and dependence on costimulation for proliferation and differentiation into cytokine-secreting cells, we isolated CD4$^+$CD44$^+$CD25$^-$CD62L$^-$ cells from the spleen and lymph nodes. Purified cells were labeled with CFSE and stimulated for 16 h with immobilized CD3ε antibodies in the absence of costimulation as suboptimal stimulus. Stimulated cells were cultured in medium alone or medium containing IL-2, IL-7, or IL-15 and followed by analysis for cell division (31). *Crt*$^{+/+}$ cells did not proliferate in response to suboptimal CD3 triggering, whereas the same stimulus was sufficient to determine significant expansion of *crt*$^{-/-}$ cells (Fig. 5 b). IL-2 and IL-7 further implemented this cell proliferation, whereas IL-15 was without any effect, as expected for murine CD4$^+$ memory cells (32). Stimulation with CD3 and CD28 antibodies for 40 h promoted increased responses in *crt*$^{-/-}$ effector–memory T cells; nevertheless, we detected robust proliferation of both *crt*$^{-/-}$ and *crt*$^{+/+}$ effector–memory T cells that was not significantly influenced by cytokine addition (Fig. 5 b). Analysis of CFSE dilution and annexin V staining at different times after CD3ε stimulation without CD28 revealed increased percentages of proliferating cells as well as reduced percentages of apoptotic cells in *crt*$^{-/-}$ samples when compared with *crt*$^{+/+}$ samples. In contrast, no differences between *crt*$^{-/-}$ and *crt*$^{+/+}$ samples were

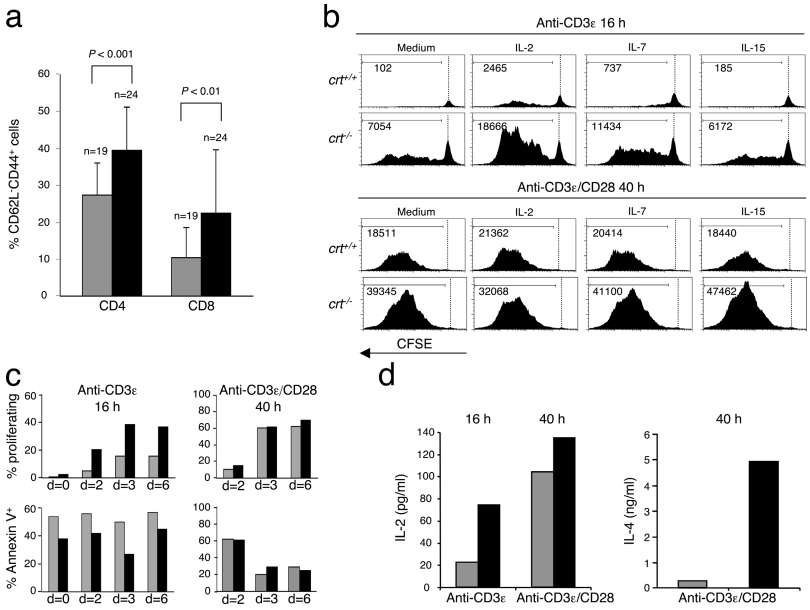

Figure 5. Augmented representation of effector–memory T cells in *crt*$^{-/-}$ chimeras and in vitro responsiveness to suboptimal CD3ε stimulation. (a) Relative representations of CD44^{+}CD62L^{-} cells in CD4^{+} and CD8^{+} subsets. Gray bars, *crt*$^{+/+}$ chimeras; black bars, *crt*$^{-/-}$ chimeras. (b) CFSE dilution in purified CD4^{+} effector–memory cells stimulated with CD3ε mAb for 16 h (top) and CD3ε+CD28 mAbs for 40 h (bottom) as detailed in Materials and methods. The addition of a particular cytokine is indicated on top of the relative histograms. Numbers indicate the absolute values of cells recovered within the marker limits in standardized acquisitions. (c) Relative representations at different time points of effector–memory T cells with diluted CFSE (i.e., proliferating; top) and cells positive for annexin V (bottom) upon stimulation with the indicated mAbs for the indicated times. (d) IL-2 and IL-4 concentrations in culture supernatants of effector–memory T cells stimulated with the indicated mAbs for the indicated times. Gray bars, *crt*$^{+/+}$ chimeras; black bars, *crt*$^{-/-}$ chimeras.

detected when cells were stimulated with CD3ε and CD28 antibodies (Fig. 5 c). Analysis of IL-2 secretion after suboptimal TCR stimulation revealed a prominent increase in *crt*$^{-/-}$ versus *crt*$^{+/+}$ cells (Fig. 5 d). These results indicate that effector–memory T cells from *crt*$^{-/-}$ chimeras display a lower activation threshold and less dependence on costimulation to mount a productive response. Furthermore, quantification of IL-4 in the supernatant of effector–memory T cells stimulated with CD3ε and CD28 antibodies revealed a prominent increase of IL-4 production in *crt*$^{-/-}$ cultures (Fig. 5 d).

Induction of unresponsiveness in *crt*$^{-/-}$ T cells

Induction of T cell unresponsiveness or anergy is supposed to play an important role in maintaining peripheral tolerance (33). Anergy can be induced in vitro through a massive increase in cytosolic Ca^{2+} before T cell stimulation (34). Therefore, we tested whether sorted effector–memory T cells from FLP chimeras became unresponsive to TCR stimulation after pretreatment with ionomycin (Supplemental Materials and methods). Fig. 6, a and b, shows the results of two independent experiments in which either untreated or ionomycin-pretreated cells were stimulated with CD3ε antibodies. Both cell proliferation scored by CFSE dilution or [^{3}H]thymidine incorporation and IL-2 production in *crt*$^{-/-}$ cells were significantly inhibited by ionomycin pretreatment with a relative efficiency undistinguishable from that observed with *crt*$^{+/+}$ cells. To further substantiate this phenomenon in vivo, we fed DO11.10tg mice with OVA (100 mg/day) for 5 d to assess anergy induction, as described previously (34). Sorted CD4 cells from untreated or OVA-fed mice were stimulated in vitro with DCs pulsed with decreasing doses of OVAp. Fig. 6 c shows that both [^{3}H]thymidine incorporation and IL-2 production were significantly reduced in *crt*$^{-/-}$ cells from OVA-fed animals, implying that unresponsiveness could be enforced in *crt*$^{-/-}$ cells.

Deregulated signal transduction in *crt*$^{-/-}$ T cells

To investigate whether CRT deficiency affected Ca^{2+} signaling in T cells, sorted CD4^{+} effector–memory cells were loaded with fura-2 and analyzed by single cell calcium imaging (Supplemental Materials and methods). Stimulation with CD3ε antibodies was followed by capacitive calcium entry in both *crt*$^{-/-}$ and *crt*$^{+/+}$ cells, thus indicating that ER calcium release and Ca^{2+} release–activated Ca^{2+} channel activation function normally in both cell types. Interestingly, increased frequencies of responding *crt*$^{-/-}$ versus *crt*$^{+/+}$ cells (48.4 ± 5%, $n = 120$ vs. 39.5 ± 4%, $n = 156$) were observed, indicating that the threshold for activation of individual cells may be lowered by CRT deficiency. Because ex vivo cells did not allow prolonged analyses, we performed a more detailed investigation of Ca^{2+} signaling with OVAp-specific T helper clones derived from DO11.10tg chimeras. Three different clones for each group of *crt*$^{-/-}$ and *crt*$^{+/+}$ chimeras stimulated with CD3ε antibodies displayed increased frequencies

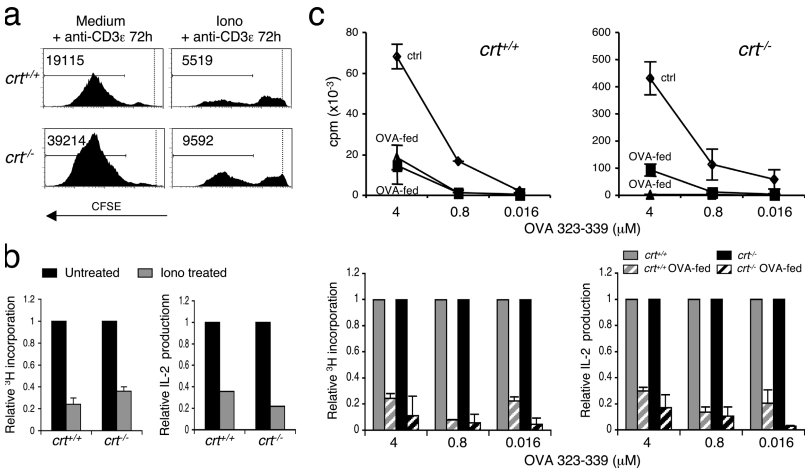

Figure 6. In vitro and in vivo induction of anergy in *crt*$^{-/-}$ CD4 cells. (a) CFSE dilution in purified CD4 effector–memory cells treated with 1 μM ionomycin and then stimulated with CD3ε mAb for 72 h. FACS analysis was performed 3 d later. Numbers indicate the absolute values of cells recovered within the marker limits in standardized acquisitions. One experiment representative of three is shown. (b) Relative [^{3}H]thymidine incorporations (left) and IL-2 concentration in culture supernatants (right) of effector–memory T cells either untreated or treated with 1 μM ionomycin upon stimulation with the CD3ε and CD28 mAbs for 96 h. (c) [^{3}H]thymidine incorporation in purified CD4$^+$ DO11.10tg T cells from untreated (ctrl) or OVA-fed chimeras of the indicated genotype stimulated for 96 h with DCs loaded with decreasing concentrations of OVAp (top panels). The displayed results are representative of three different experiments. Relative [^{3}H]thymidine incorporation (bottom left) and IL-2 concentration in culture supernatants (bottom right) of CD4$^+$ DO11.10tg T cells stimulated with DCs loaded with the indicated concentrations of OVAp for 96 h. Mean ± SD of three different OVA-fed DO11.10tg *crt*$^{+/+}$ (gray dashed bars) and *crt*$^{-/-}$ (black dashed bars) chimeric mice are shown.

of responding *crt*$^{-/-}$ versus *crt*$^{+/+}$ cells as observed with ex vivo–isolated effector–memory cells (Fig. 7 a). Although the most common pattern of response observed in CD3ε-stimulated *crt*$^{+/+}$ cells was a single $[Ca^{2+}]_i$ spike followed by a sustained, slowly decreasing phase of $[Ca^{2+}]_i$ elevation, repetitive $[Ca^{2+}]_i$ elevations leading to an oscillatory pattern were more frequently detected in *crt*$^{-/-}$ cells (Fig. 7 b). Indeed, in *crt*$^{-/-}$ clones fewer cells responding to the stimulus with only one or two $[Ca^{2+}]_i$ spikes were detected over the time frame of analysis with respect to *crt*$^{+/+}$ clones. Also, cells responding to the stimulus with six or more $[Ca^{2+}]_i$ spikes were only detected in *crt*$^{-/-}$ clones (Fig. 7 c). Comparable $[Ca^{2+}]_i$ patterns were observed when the same T cell clones were stimulated with OVA-loaded DCs (not depicted).

Because oscillatory $[Ca^{2+}]_i$ elevations efficiently induce NFAT dephosphorylation and nuclear translocation (13), we analyzed NFAT dephosphorylation and nuclear translocation in *crt*$^{-/-}$ as well as *crt*$^{+/+}$ T helper clones at different times after CD3ε stimulation. Of the three calcium-regulated NFAT members expressed in T cells (NFAT1, NFAT2, and NFAT4), NFAT1 is highly expressed at baseline (35) and its activation by TCR signaling is relatively short-lived. In fact, the bulk of activated NFAT1 reverts to a phosphorylated, cytoplasmic form within a few hours of stimulation (36). This effect is mediated by NFAT nuclear export kinases such as glycogensynthase kinase-3 (37), which is inhibited in CD3-stimulated human T cells by CD28 costimulation (38). 30 min after CD3 cross-linking with avidin, NFAT1 was efficiently dephosphorylated and translocated to the nucleus in both *crt*$^{+/+}$ and *crt*$^{-/-}$ clones. At 3 h after stimulation, in *crt*$^{+/+}$ cells NFAT1 was found in the cytosol mainly in its phosphorylated forms, as described previously (36), whereas in *crt*$^{-/-}$ cells faster migrating dephosphorylated NFAT1 was still detectable. At 16 h after stimulation, dephosphorylated NFAT1 could be detected in the cytosol only upon prolonged exposure of *crt*$^{-/-}$ blots, but a prominent band corresponding to dephosphorylated NFAT1 was readily detected in the nuclear fraction of *crt*$^{-/-}$ but not *crt*$^{+/+}$ T cell clones (Fig. 8 a). The prolonged nuclear translocation of NFAT1 in *crt*$^{-/-}$ T helper clones may be the result of different calcium signaling between *crt*$^{+/+}$ and *crt*$^{-/-}$ cells. Stimulation of T helper clones with DCs loaded with decreasing doses of OVAp revealed in *crt*$^{-/-}$ cells a dose-dependent decrease in NFAT1 nuclear translocation at 16 h after activation, whereas the same low amount of NFAT1 was recovered from nuclear fractions of *crt*$^{+/+}$ cells regardless of the OVAp concentration used for stimulation (Fig. 8 b). These data further confirm the lower threshold of activation in *crt*$^{-/-}$ cells and suggest that CRT deficiency positively influences NFAT activation after TCR stimulation.

Nuclear translocation of NFAT1 may trigger the transcription of genes involved in T cell activation as well as genes leading to tolerance and anergy (39). A requisite for the productive immune response consists in the parallel activation of mitogen-activated protein kinases (MAPKs), their nuclear translocation, and phosphorylation of specific transcription factors, which regulate together with NFAT the transcription of genes involved in T cell activation. Therefore, we investigated p38MAPK, ERK, and jun phosphorylation in T helper clones stimulated with CD3 antibodies. At early time points

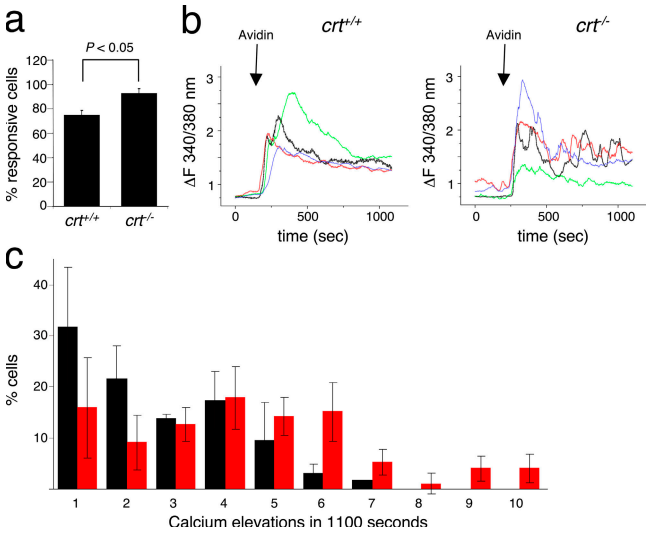

Figure 7. Recurrent calcium elevations in $crt^{-/-}$ T cell clones. $CD4^+$ DO11.10tg T cell clones from $crt^{+/+}$ and $crt^{-/-}$ chimeras were loaded with Fura-2 and monitored for changes in $[Ca^{2+}]_i$. (a) Percentages of $crt^{+/+}$ and $crt^{-/-}$ T cell clones responding with $[Ca^{2+}]_i$ elevations upon CD3ε stimulation (means ± SD of at least 97 single cells). (b) Temporal analysis of $[Ca^{2+}]_i$ elevations upon CD3 stimulation of representative $crt^{+/+}$ and $crt^{-/-}$ clones. (c) Relative distributions of cells with respect to numbers of $[Ca^{2+}]_i$ elevations over 1,100 s. Means ± SD of three independent experiments with two different clones per group. Black bars, $crt^{+/+}$, $n = 89$; red bars, $crt^{-/-}$, $n = 93$.

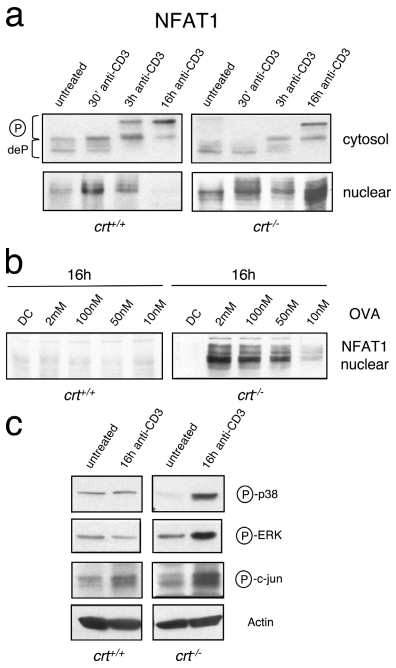

Figure 8. Protracted NFAT activation and MAPK signaling in $crt^{-/-}$ T cell clones. (a) Immunoblot analysis of NFAT1 in cytosolic and nuclear fractions of $crt^{+/+}$ and $crt^{-/-}$ DO11.10tg T cell clones stimulated with CD3ε mAb for the indicated times. The experiment is representative of three different clones per group. (b) Immunoblot of NFAT1 in nuclear fractions of $crt^{+/+}$ and $crt^{-/-}$ DO11.10tg T cell clones stimulated for 16 h with DCs loaded with decreasing doses of OVAp. The result is representative of three experiments with two different clones per group. (c) Immunoblot of phosphorylated p38MAPK, ERK, and c-jun in $crt^{+/+}$ and DO11.10tg T cell clones before and 16 h after $crt^{-/-}$ stimulation. The result is representative of four different experiments with at least two different clones.

after stimulation we did not detect differences in the phosphorylation intensities (not depicted). However, at 16 h after stimulation although c-jun was analogously phosphorylated in both $crt^{+/+}$ and $crt^{-/-}$ clones, more intensely phosphorylated p38MAPK and ERK could be detected in $crt^{-/-}$ compared with $crt^{+/+}$ T helper clones, implying a more sustained activation of these MAPK pathways (Fig. 8 c). Collectively, these results support the view that CRT critically participates in the regulation of TCR-dependent gene transcription during an adaptive immune response.

DISCUSSION

CRT is a molecular chaperone and the main Ca^{2+} buffering protein in the ER. In vivo as well as in vitro studies with $crt^{-/-}$ cells have demonstrated the crucial role of CRT in the homeostasis of intracellular Ca^{2+}, thereby regulating signal transduction and cell susceptibility to apoptosis (18, 19). However, the role CRT might play in TCR-mediated signaling was not investigated so far. Here we showed that RAG/γ chain DKO mice reconstituted with $crt^{-/-}$ FLPs displayed blepharitis and alopecia, two phenotypic traits that were correlated with immunopathological T cell activation (40, 41). CRT deletion could also influence the function of other immune cells. Indeed, it was shown to bind to the collectin family of molecules (C1q, the first subcomponent of complement, and surfactant proteins A and D; reference 42), and this binding was shown to influence inflammatory processes (43). Recently, CRT at the cell surface was implicated in inducing the clearance of apoptotic cells (44). The role of T cells in determining the phenotype of $crt^{-/-}$ chimeras was supported by the absence of any sign of disease at week 20 after reconstitution in chimeras generated with $crt^{-/-}/cd3\varepsilon^{-/-}$ DKO FLPs, in which $crt^{-/-}$ T cells were absent, whereas 100% of $crt^{-/-}$ chimeras displayed overt immunopathology at week 10 after reconstitution. Two crucial mechanisms limit the harmful potential of peripheral T cells for the organism; namely, the deletion of self-reactive T cells during thymic differentiation and the immunosuppressive competence of the $CD4^+CD25^+$ T reg cell subset. Analysis of apoptosis of $CD4^+8^+$ DP cells did not reveal an impairment of $crt^{-/-}$ thymocytes to undergo antigen-driven clonal deletion, thereby suggesting that tolerance induction through this mechanism was not implicated. The capacity of $crt^{-/-}$ T reg cells to inhibit a CD3-driven mitogenic response was not impaired, ruling out an intrinsic defect of this cell subset in determining the immunopathological damage. However, $crt^{-/-}$ CD4 T cells were less sensitive to inhibition by T reg cells. Nevertheless, antinuclear, anti–double-stranded DNA, and anti-cardiolipin

antibodies were not detected in the sera from $crt^{-/-}$ chimeras, suggesting that an autoreactive response was not implicated in the observed immunopathology. Analysis of peripheral T cell compartments revealed increased frequencies of T cells displaying markers of activation and secreting proinflammatory cytokines as well as expansion of the $CD44^+CD62L^-$ effector–memory subset in mice reconstituted with $crt^{-/-}$ FLPs. Chimeric mice generated with $crt^{-/-}$ DO11.10tg FLPs did not display an overt pathological phenotype as "polyclonal" mice up to 24 wk after reconstitution. Peripheral colonization of lymphopenic hosts by T cells determines homeostatic expansion of positively selected T cells and a pattern of gene expression similar to that of antigen-experienced cells (45) with acquisition of the $CD44^+62L^-$ phenotype (46). Because in DO11.10tg mice a fraction of peripheral T cells does not express the clonotypic TCR but TCRs with different specificities, we compared the representation of $CD44^+62L^-$ cells either expressing or not the transgenic TCR. $Crt^{-/-}$ and $crt^{+/+}$ chimeras did not display significant differences in $CD44^+62L^-$ expression in the clonotype-positive compartment ($crt^{+/+}$ = 37.2 ± 11.4%, n = 4; $crt^{-/-}$ = 38.7 ± 12.2%, n = 4); however, a significant difference in $CD44^+62L^-$ cell representation was detected in the clonotype-negative fraction ($crt^{+/+}$ = 39.0 ± 6.2%, n = 4; $crt^{-/-}$ = 54.8 ± 7.5%, n = 4, P = 0.006), thereby suggesting that CRT deletion altered the T cell response to environmental antigens but not homeostatic expansion. Moreover, this indicates that immunopathology in $crt^{-/-}$ chimeras depends on hyperresponsiveness to environmental antigens of a physiological peripheral T cell pool. Indeed, antigen priming of DO11.10tg $crt^{-/-}$ cells determined exaggerated swelling of the draining lymph node as well as more robust cell proliferation and cytokine secretion than observed with the $crt^{+/+}$ counterpart. These results were consistent with the reduced apoptosis and increased IL-2 production by suboptimally stimulated $crt^{-/-}$ T cells, suggesting that the threshold for TCR activation was lowered and persistence of positive signals was enforced in peripheral T cells by CRT deficiency.

Calcium signaling intervenes at multiple stages during T cell development in the thymus; e.g., thymocyte β selection by the pre-TCR (24) and positive as well as negative selection by the αβTCR (25–27). Moreover, the sustained $[Ca^{2+}]_i$ elevation after TCR triggering of peripheral T cells is crucial for the development of the immune response (11). CRT deficiency affected T cell function manifestly in the periphery while thymocyte development appeared unaltered. In spite of analogous signal transduction pathways used by both immature and mature T cells, the magnitude of the $[Ca^{2+}]_i$ increase after TCR stimulation is larger in mature T cells (references 24 and 25, and unpublished data). We hypothesize that CRT deficiency selectively affects Ca^{2+} signaling when sustained $[Ca^{2+}]_i$ elevations are critical in the regulation of the T cell response, likely in the peripheral T cell upon antigen encounter. After TCR stimulation, we observed repetitive $[Ca^{2+}]_i$ peaks leading to an oscillatory pattern in $crt^{-/-}$ cells, whereas sustained Ca^{2+} influx predominated in $crt^{+/+}$ T cells. Similar observations were made in *Xenopous* oocytes, where CRT was proposed to regulate the sarco-endoplasmic reticulum calcium transport ATPase (SERCA), which pumps Ca^{2+} from the cytosol into the ER lumen, thereby influencing the degree of ER Ca^{2+} filling (47). Indeed, CRT association with SERCA reduced pump activity through the recruitment of the ER oxidoreductase ERp57 and oxidation of critical ER facing thiol groups of SERCA (47, 48). An increased activity of the SERCA pump might contribute to the oscillatory $[Ca^{2+}]_i$ pattern observed in $crt^{-/-}$ T cells.

Magnitude, kinetics, and subcellular location of Ca^{2+} signal can all be deciphered by the cell and translated into distinct responses, thereby conferring specificity to an otherwise pleiotropic signal (49). Indeed, $[Ca^{2+}]_i$ oscillation frequency was shown to control the activation of distinct sets of transcription factors and the expression of different genes (12, 13). $[Ca^{2+}]_i$ spikes elicited by CD3ε antibodies were positively correlated with NFAT-regulated gene expression (50). Recently, oscillatory changes in $[Ca^{2+}]_i$ were shown to be more efficient than a continuous increase in translocating NFAT (13). CD3ε stimulation of T cell clones derived from DO11.10tg $crt^{-/-}$ chimeric mice resulted in the reduced detection of phosphorylated NFAT1 forms in the cytosol and the prominent accumulation of dephosphorylated forms in the nucleus, suggesting that the strength of TCR signaling was enhanced in $crt^{-/-}$ cells and nuclear export kinase activity was inhibited. Similar results were obtained in the same clones stimulated with the cognate antigen presented by DCs, thus suggesting that enhanced IL-2 secretion in $crt^{-/-}$ cells could depend on aberrant NFAT regulation.

The analysis of the T cell response after sustained $[Ca^{2+}]_i$ elevation by ionomycin treatment revealed the Ca^{2+}-dependent up-regulation of genes involved in the targeted proteolysis of signaling proteins. This transcriptional program is controlled by calcineurin/NFAT activation and induces T cell unresponsiveness to TCR stimulation (51). Deletion of these genes in mice results in immunopathology, suggesting the physiological relevance of such a transcriptional program in T cell homeostasis. Treatment of $crt^{-/-}$ effector–memory T cells with ionomycin promoted unresponsiveness to subsequent TCR stimulation and OVA feeding of DO11.10tg chimeras promoted ex vivo T cell unresponsiveness of sorted $crt^{-/-}$ $CD4^+$ cells, suggesting that CRT deficiency was not altering the functional efficiency of the inhibitory machinery implicated in inducing T cell unresponsiveness but maybe interferes with its up-regulation after TCR stimulation. CRT could ensure the appropriate supply of Ca^{2+} for the physiological calcium response and regulated T cell activation. Interestingly, it was shown that calcium restriction in kidney epithelial cells was associated with increased B-Raf protein levels and derepressed B-Raf/ERK pathways leading to phenotypic remodeling and conversion to cell proliferation of otherwise growth-inhibited cells (52). The more oscillatory calcium response observed in $crt^{-/-}$ cells could result in a different transcriptional program in which activation components would dominate. Positive

regulators of TCR-induced activation include p38MAPK, ERK, and jun (53). These proteins were shown to influence the NFAT transactivation potential, further contributing to the T cell activation genetic program controlled by NFAT (39, 54, 55). Analysis of p38MAPK, ERK, and jun phosphorylation after TCR stimulation revealed significantly protracted activation of p38MAPK and ERK in *crt*$^{-/-}$ clones, implying a defective modulation of these T cell activation pathways in the absence of CRT. Accordingly, $[Ca^{2+}]_i$ oscillations were shown to reduce the threshold for Ras activation potentiating ERK activation induced by suboptimal agonist concentration (56).

crt$^{-/-}$ chimeras were characterized histologically by normal thymus, gut, kidney, liver, and pancreas. Inflammatory infiltrates were evident in the skin and in the peribronchial space of the lung. Furthermore, IgG_1 and IgE levels were significantly increased. These features of *crt*$^{-/-}$ chimeras are reminiscent of NFAT1/4 DKO mice described by Ranger et al. (41), in which the unbalanced activation of NFAT2 induced up-regulation of Th2-dependent cytokine responses. Another study demonstrated that NFAT1 and NFAT2 were necessary for TCR-mediated T cell effector functions, suggesting that the functions of NFAT1 and NFAT2 may be largely redundant in the regulation of most effector cytokines (57) and indicating that NFAT1 might participate with NFAT2 in the generation of T cell effector functions. The phenotype of *crt*$^{-/-}$ chimeras could derive from a dominance of Th2 differentiation in vivo resulting from hyperresponsiveness to TCR stimulation (58). Indeed, considerable amounts of IL-4 were detected in the supernatants of *crt*$^{-/-}$ but not *crt*$^{+/+}$ primary T cells stimulated with CD3 and CD28 antibodies. In conclusion, our study suggests that CRT modulates T cell activation by regulating calcium signaling. CRT deficiency results in a lower stimulation threshold, enhanced TCR signaling through MAPK pathways, and protracted NFAT activation in peripheral T cells, thereby endowing the adaptive T cell response with harmful potential for the organism.

MATERIALS AND METHODS

Mice. *crt*$^{+/-}$ (H-2^b) mice (20), BALB/c RAG/γ chain DKO (H-2^d) mice provided by M. Ito (Central Institute for Experimental Animals, Miyamae, Kawasaki, Japan), B6D2F1 (BALB/c × C57BL/6 F_1, H2$^{d/b}$) mice from Charles River Germany, and transgenic DO11.10 (H-2^d) mice from The Jackson Laboratory were bred and treated in accordance with the Swiss Federal Veterinary Office guidelines. Experiments were approved by "Dipartimento della Sanità e della Socialità." To generate fetal liver chimera, timed pregnant *crt*$^{+/-}$ female mice were killed at day 13 p.c. and the embryos were explanted under sterile conditions (genotype frequencies were as follows: *crt*$^{-/-}$, 16%; *crt*$^{+/+}$, 31%; *crt*$^{+/-}$, 53%; n = 553). The following two sets of primers were used to screen the progeny: 5′-CTCCAGGTCCCCGTAAAATTTGCC-3′ and 5′-AGGTCTAAACCAGTCAAAAGGACC-3′ for the detection of the *crt* WT gene and 5′-TCGTGCTTTACGGTATCGCCGCTCCCGATT-3′and5′-CGCGGATCCACCTCCCATGACAGCCATTTA-3′ for identification of the *crt* mutant gene. RAG/γ chain DKO at 6 wk of age were used as recipients for lymphoid reconstitution. Mice were irradiated with 4 Gy from a ^{137}Cs source (Biobeam 8000; STS GmbH) at 3.75 Gy/min. Mice were i.v. injected with 2 × 10^6 fetal liver cells in 200 μl PBS. TNF-α in sera was quantified with an ELISA kit (Quantikine; R&D Systems). To generate *crt*$^{+/-}$/DO11.10tg mice, *crt*$^{+/-}$ mice were crossed with DO11.10tg mice and the progeny was screened for *crt* mutation as described above and for the TCR transgene with the following primers: 5′-CAGGAGGGATCCAGTGCCAGC-3′ and 5′-TGGCTCTACAGTGAGTTTGGT-3′. H-2$^{b/d}$ *crt*$^{-/-}$ and *crt*$^{+/+}$ DO11.10tg embryos from F_1 intercrosses were identified for *crt* and TCR transgene with the PCRs described above and for H-2 haplotype by generating DCs from fetal livers in the presence of recombinant granulocyte-macrophage colony-stimulating factor (R&D Systems), and by flow cytometry of the in vitro–generated DCs with CD11c and H-2–specific antibodies.

T cell purification and proliferation assays. T cells were isolated from peripheral lymph nodes and spleens by negative selection with immunomagnetic beads followed by cells sorting. Cells were incubated with biotin-conjugated anti-CD19, anti-Ter119, anti-panNK, and anti-CD11b mAbs (eBioscience). T lymphocytes were enriched by removing biotin-labeled cells bound to streptavidin-conjugated magnetic beads. CD4$^+$ naive (CD4$^+$CD44$^-$CD25$^-$CD62L$^+$) and effector–memory (CD4$^+$CD44$^+$CD25$^-$CD62L$^-$) T cell subsets were sorted with a FACSAria (Becton Dickinson). The cells were labeled with CFSE (Invitrogen) and stimulated with 10 μg/ml of plate-bound anti-CD3ε mAb with or without 5 μg/ml of coimmobilized anti-CD28 mAb (eBioscence). At different times, we transferred effector–memory cells to uncoated wells to terminate TCR stimulation and continued cell culture for 96 h in medium alone or in the presence of 90 U/ml IL-2, 25 ng/ml IL-7, or 25 ng/ml IL-15, as described previously (31). FACS acquisitions were standardized by fixed numbers of calibration beads (BD Biosciences). IL-2 was measured in supernatants with an ELISA kit according to the manufacturer's instructions (Quantikine; R&D Systems). CD4$^+$ naive T cell proliferation was scored on sorted cells that were cultured in anti-CD3ε–coated flat-bottom microplates at 3 × 10^4 cells/well for 96 h. [^{3}H]thymidine (2 μCi/well) was added and the plates were harvested after 12 h of incubation. Bone marrow–derived DCs were generated from femurs of mice in the presence of recombinant granulocyte-macrophage colony-stimulating factor (R&D Systems). Sorted CD4$^+$ naive T cells from DO11.10tg mice were cultured at 10 DO11.10tg cells to 1 DC ratio with DCs pulsed with various doses of $OVA_{323–339}$ peptide. For adoptive transfer of TCR transgenic cells, spleen and lymph node cells from RAG/γ chain DKO chimeric mice reconstituted with either *crt*$^{+/+}$ or *crt*$^{-/-}$ DO11.10tg H-2$^{b/d}$ progenitors were labeled with CFSE. Cell suspensions containing 10^6 TCR transgenic cells were i.v. injected into B6D2F1 mice. Adoptively transferred mice were immunized s.c. into the footpad 24 or 48 h later with 2 × 10^6 DCs pulsed with 2 μM $OVA_{323–339}$ peptide at 37°C for 1 h. Popliteal lymph nodes were analyzed at various times after immunization for cell number and cytokine secretion by DO11.10tg cells.

T reg cell inhibition assay. CD4$^+$ T reg cells (CD4$^+$CD25$^+$) and CD4$^+$ naive T cells (CD4$^+$CD25$^-$CD62L$^+$) were isolated from peripheral lymph nodes and spleens by negative selection with immunomagnetic beads followed by cell sorting as described above. Naive CD4$^+$ T cell were cocultured in 96-well round-bottom plates at 50,000 cells/well with serial dilutions of T reg cells (from 1:1 to 1:64) in the presence of 5,000 DCs/well and with 0.2 μg/ml anti-CD3ε mAb. After 48 h of incubation [^{3}H]thymidine (2 μCi/well) was added and the plates were harvested after 12 h of incubation.

Biochemical procedures. CD4$^+$ DO11.10tg T cell clones were generated from the spleens of *crt*$^{-/-}$ and *crt*$^{+/+}$ DO11.10tg chimeras by stimulation with OVAp-loaded DCs. They were restimulated with OVAp-loaded DCs every 14 d. For CD3 stimulation, clones at days 10–13 from restimulation were incubated for 30 min at room temperature with 1 μg/ml biotinylated CD3ε mAb (clone 145-2C11) in cell culture medium. Unbound antibody was removed by centrifugation and the cells were resuspended in medium containing 1 μg/ml avidin for 30 min to 16 h as indicated in Results. In some experiments, T cell clones were stimulated with OVAp-loaded DCs at a ratio of 20:1. For biochemical analysis, cells were washed twice in PBS and lysed in a hypo-osmotic buffer (10 mM Hepes, 1.5 mM $MgCl_2$, 10 mM KCl, 0.05% NP-40, and protease inhibitors) for 10 min on ice. The nuclei were separated from the cytosolic fraction by a 10-min centrifugation at 2,000 *g*. Samples were analyzed by SDS PAGE followed by immunoblot. NFAT1

antibodies were provided by N.R. Rice (NCI-Frederick Cancer Research and Development Center, Frederick, MD), phospho-p38 MAPK (3D7) and phospho-ERK (197G2) rabbit mAbs were from Cell Signaling Technology, phospho-c-jun (KM-1) mouse mAb was from Santa Cruz Biotechnology, Inc., and β actin mouse mAb (A-5441) was from Sigma-Aldrich.

Online supplemental material. Supplemental Results and Figs. S1 and S2 show unaltered pre-TCR signaling as well as unaltered positive selection and deletion of $crt^{-/-}$ thymocytes. Supplemental Materials and methods describe the detection of autoantibodies, mAbs used in flow cytometry, induction of anergy, and calcium imaging. Supplemental Results, Materials and methods, and Fig. S1 are available at http://www.jem.org/cgi/content/full/jem.20051519/DC1.

We thank Dr. Mamoru Ito (Laboratory of Immunology, CIEA, Kawasaki, Japan) for providing RAG/γ chain DKO mice, Dr. Nancy R. Rice and Mimi Ernst (NCI-Frederick Cancer Research and Development Center. Frederick, MD) for the generous supply of anti-NFAT1 serum, Enrica Mira-Catò for intragastric administration of OVA, David Jarrossay for FACS sorting, and Consuelo Anzilotti and Paola Migliorini (School of Medicine, University of Pisa) for support in autoantibody detection.

This work was supported by grants to F. Grassi from the Leukemia and Lymphoma Society, Swiss National Science Foundation, Fondazione Ticinese per la Ricerca sul Cancro, and Fondazione per la Ricerca sulla Trasfusione e sui Trapianti. U. Schenk is a recipient of a fellowship from the Novartis Foundation.

The authors have no conflicting financial interests.

Submitted: 28 July 2005
Accepted: 20 January 2006

REFERENCES

1. Veillette, A., S. Latour, and D. Davidson. 2002. Negative regulation of immunoreceptor signaling. *Annu. Rev. Immunol.* 20:669–707.
2. Tsui, H.W., K.A. Siminovitch, L. de Souza, and F.W. Tsui. 1993. Motheaten and viable motheaten mice have mutations in the haematopoietic cell phosphatase gene. *Nat. Genet.* 4:124–129.
3. Shultz, L.D., P.A. Schweitzer, T.V. Rajan, T. Yi, J.N. Ihle, R.J. Matthews, M.L. Thomas, and D.R. Beier. 1993. Mutations at the murine motheaten locus are within the hematopoietic cell protein-tyrosine phosphatase (Hcph) gene. *Cell.* 73:1445–1454.
4. Bachmaier, K., C. Krawczyk, I. Kozieradzki, Y.Y. Kong, T. Sasaki, A. Oliveira-dos-Santos, S. Mariathasan, D. Bouchard, A. Wakeham, A. Itie, et al. 2000. Negative regulation of lymphocyte activation and autoimmunity by the molecular adaptor Cbl-b. *Nature.* 403: 211–216.
5. Chiang, Y.J., H.K. Kole, K. Brown, M. Naramura, S. Fukuhara, R.J. Hu, I.K. Jang, J.S. Gutkind, E. Shevach, and H. Gu. 2000. Cbl-b regulates the CD28 dependence of T-cell activation. *Nature.* 403:216–220.
6. Greenwald, R.J., G.J. Freeman, and A.H. Sharpe. 2005. The B7 family revisited. *Annu. Rev. Immunol.* 23:515–548.
7. Brunkow, M.E., E.W. Jeffery, K.A. Hjerrild, B. Paeper, L.B. Clark, S.A. Yasayko, J.E. Wilkinson, D. Galas, S.F. Ziegler, and F. Ramsdell. 2001. Disruption of a new forkhead/winged-helix protein, scurfin, results in the fatal lymphoproliferative disorder of the scurfy mouse. *Nat. Genet.* 27:68–73.
8. Lin, L., M.S. Spoor, A.J. Gerth, S.L. Brody, and S.L. Peng. 2004. Modulation of Th1 activation and inflammation by the NF-κB repressor Foxj 1. *Science.* 303:1017–1020.
9. Sakaguchi, N., T. Takahashi, H. Hata, T. Nomura, T. Tagami, S. Yamazaki, T. Sakihama, T. Matsutani, I. Negishi, S. Nakatsuru, and S. Sakaguchi. 2003. Altered thymic T-cell selection due to a mutation of the ZAP-70 gene causes autoimmune arthritis in mice. *Nature.* 426:454–460.
10. Lenardo, M., K.M. Chan, F. Hornung, H. McFarland, R. Siegel, J. Wang, and L. Zheng. 1999. Mature T lymphocyte apoptosis—immune regulation in a dynamic and unpredictable antigenic environment. *Annu. Rev. Immunol.* 17:221–253.
11. Lewis, R.S. 2001. Calcium signaling mechanisms in T lymphocytes. *Annu. Rev. Immunol.* 19:497–521.
12. Dolmetsch, R.E., K. Xu, and R.S. Lewis. 1998. Calcium oscillations increase the efficiency and specificity of gene expression. *Nature.* 392:933–936.
13. Tomida, T., K. Hirose, A. Takizawa, F. Shibasaki, and M. Iino. 2003. NFAT functions as a working memory of Ca^{2+} signals in decoding Ca^{2+} oscillation. *EMBO J.* 22:3825–3832.
14. Crabtree, G.R., and E.N. Olson. 2002. NFAT signaling: choreographing the social lives of cells. *Cell.* 109:S67–S79.
15. Hogan, P.G., L. Chen, J. Nardone, and A. Rao. 2003. Transcriptional regulation by calcium, calcineurin, and NFAT. *Genes Dev.* 17:2205–2232.
16. Ellgaard, L., and A. Helenius. 2003. Quality control in the endoplasmic reticulum. *Nat. Rev. Mol. Cell Biol.* 4:181–191.
17. Krause, K.H., and M. Michalak. 1997. Calreticulin. *Cell.* 88:439–443.
18. Pinton, P., D. Ferrari, E. Rapizzi, F. Di Virgilio, T. Pozzan, and R. Rizzuto. 2001. The Ca^{2+} concentration of the endoplasmic reticulum is a key determinant of ceramide-induced apoptosis: significance for the molecular mechanism of Bcl-2 action. *EMBO J.* 20:2690–2701.
19. Nakamura, K., E. Bossy-Wetzel, K. Burns, M.P. Fadel, M. Lozyk, I.S. Goping, M. Opas, R.C. Bleackley, D.R. Green, and M. Michalak. 2000. Changes in endoplasmic reticulum luminal environment affect cell sensitivity to apoptosis. *J. Cell Biol.* 150:731–740.
20. Mesaeli, N., K. Nakamura, E. Zvaritch, P. Dickie, E. Dziak, K.H. Krause, M. Opas, D.H. MacLennan, and M. Michalak. 1999. Calreticulin is essential for cardiac development. *J. Cell Biol.* 144:857–868.
21. Lynch, J., L. Guo, P. Gelebart, K. Chilibeck, J. Xu, J.D. Molkentin, L.B. Agellon, and M. Michalak. 2005. Calreticulin signals upstream of calcineurin and MEF2C in a critical Ca^{2+}-dependent signaling cascade. *J. Cell Biol.* 170:37–47.
22. Guo, L., K. Nakamura, J. Lynch, M. Opas, E.N. Olson, L.B. Agellon, and M. Michalak. 2002. Cardiac-specific expression of calcineurin reverses embryonic lethality in calreticulin-deficient mouse. *J. Biol. Chem.* 277:50776–50779.
23. Probert, L., J. Keffer, P. Corbella, H. Cazlaris, E. Patsavoudi, S. Stephens, E. Kaslaris, D. Kioussis, and G. Kollias. 1993. Wasting, ischemia, and lymphoid abnormalities in mice expressing T cell-targeted human tumor necrosis factor transgenes. *J. Immunol.* 151:1894–1906.
24. Aifantis, I., F. Gounari, L. Scorrano, C. Borowski, and H. von Boehmer. 2001. Constitutive pre-TCR signaling promotes differentiation through Ca^{2+} mobilization and activation of NF-κB and NFAT. *Nat. Immunol.* 2:403–409.
25. Bhakta, N.R., D.Y. Oh, and R.S. Lewis. 2005. Calcium oscillations regulate thymocyte motility during positive selection in the three-dimensional thymic environment. *Nat. Immunol.* 6:143–151.
26. Nakayama, T., Y. Ueda, H. Yamada, E.W. Shores, A. Singer, and C.H. June. 1992. *In vivo* calcium elevations in thymocytes with T cell receptors that are specific for self ligands. *Science.* 257:96–99.
27. Freedman, B.D., Q.H. Liu, S. Somersan, M.I. Kotlikoff, and J.A. Punt. 1999. Receptor avidity and costimulation specify the intracellular Ca^{2+} signaling pattern in $CD4^+CD8^+$ thymocytes. *J. Exp. Med.* 190:943–952.
28. Murphy, K.M., A.B. Heimberger, and D.Y. Loh. 1990. Induction by antigen of intrathymic apoptosis of $CD4^+CD8^+TCR^{lo}$ thymocytes in vivo. *Science.* 250:1720–1723.
29. Sakaguchi, S., N. Sakaguchi, M. Asano, M. Itoh, and M. Toda. 1995. Immunologic self-tolerance maintained by activated T cells expressing IL-2 receptor alpha-chains (CD25). Breakdown of a single mechanism of self-tolerance causes various autoimmune diseases. *J. Immunol.* 155:1151–1164.
30. Belkaid, Y., and B.T. Rouse. 2005. Natural regulatory T cells in infectious disease. *Nat. Immunol.* 6:353–360.
31. Gett, A.V., F. Sallusto, A. Lanzavecchia, and J. Geginat. 2003. T cell fitness determined by signal strength. *Nat. Immunol.* 4:355–360.
32. Seddon, B., P. Tomlinson, and R. Zamoyska. 2003. Interleukin 7 and T cell receptor signals regulate homeostasis of CD4 memory cells. *Nat. Immunol.* 4:680–686.
33. Schwartz, R.H. 2003. T cell anergy. *Annu. Rev. Immunol.* 21:305–334.

34. Macian, F., F. Garcia-Cozar, S.H. Im, H.F. Horton, M.C. Byrne, and A. Rao. 2002. Transcriptional mechanisms underlying lymphocyte tolerance. *Cell*. 109:719–731.
35. Northrop, J.P., S.N. Ho, L. Chen, D.J. Thomas, L.A. Timmerman, G.P. Nolan, A. Admon, and G.R. Crabtree. 1994. NF-AT components define a family of transcription factors targeted in T-cell activation. *Nature*. 369:497–502.
36. Loh, C., J.A. Carew, J. Kim, P.G. Hogan, and A. Rao. 1996. T-cell receptor stimulation elicits an early phase of activation and a later phase of deactivation of the transcription factor NFAT1. *Mol. Cell. Biol.* 16:3945–3954.
37. Beals, C.R., C.M. Sheridan, C.W. Turck, P. Gardner, and G.R. Crabtree. 1997. Nuclear export of NF-ATc enhanced by glycogen synthase kinase-3. *Science*. 275:1930–1934.
38. Diehn, M., A.A. Alizadeh, O.J. Rando, C.L. Liu, K. Stankunas, D. Botstein, G.R. Crabtree, and P.O. Brown. 2002. Genomic expression programs and the integration of the CD28 costimulatory signal in T cell activation. *Proc. Natl. Acad. Sci. USA*. 99:11796–11801.
39. Macian, F., C. Garcia-Rodriguez, and A. Rao. 2000. Gene expression elicited by NFAT in the presence or absence of cooperative recruitment of Fos and Jun. *EMBO J.* 19:4783–4795.
40. Ellison, C.A., J.M. Fischer, K.T. HayGlass, and J.G. Gartner. 1998. Murine graft-versus-host disease in an F1-hybrid model using IFN-γ gene knockout donors. *J. Immunol.* 161:631–640.
41. Ranger, A.M., M. Oukka, J. Rengarajan, and L.H. Glimcher. 1998. Inhibitory function of two NFAT family members in lymphoid homeostasis and Th2 development. *Immunity*. 9:627–635.
42. Ghebrehiwet, B., and E.I. Peerschke. 2004. cC1q-R (calreticulin) and gC1q-R/p33: ubiquitously expressed multi-ligand binding cellular proteins involved in inflammation and infection. *Mol. Immunol.* 41:173–183.
43. Gardai, S.J., Y.Q. Xiao, M. Dickinson, J.A. Nick, D.R. Voelker, K.E. Greene, and P.M. Henson. 2003. By binding SIRPα or calreticulin/CD91, lung collectins act as dual function surveillance molecules to suppress or enhance inflammation. *Cell.* 115:13–23.
44. Gardai, S.J., K.A. McPhillips, S.C. Frasch, W.J. Janssen, A. Starefeldt, J.E. Murphy-Ullrich, D.L. Bratton, P.A. Oldenborg, M. Michalak, and P.M. Henson. 2005. Cell-surface calreticulin initiates clearance of viable or apoptotic cells through trans-activation of LRP on the phagocyte. *Cell*. 123:321–334.
45. Goldrath, A.W., C.J. Luckey, R. Park, C. Benoist, and D. Mathis. 2004. The molecular program induced in T cells undergoing homeostatic proliferation. *Proc. Natl. Acad. Sci. USA*. 101:16885–16890.
46. Li, O., P. Zheng, and Y. Liu. 2004. CD24 expression on T cells is required for optimal T cell proliferation in lymphopenic host. *J. Exp. Med*. 200:1083–1089.
47. Camacho, P., and J.D. Lechleiter. 1995. Calreticulin inhibits repetitive intracellular Ca^{2+} waves. *Cell*. 82:765–771.
48. Li, Y., and P. Camacho. 2004. Ca^{2+}-dependent redox modulation of SERCA 2b by ERp57. *J. Cell Biol.* 164:35–46.
49. Berridge, M.J., M.D. Bootman, and P. Lipp. 1998. Calcium—a life and death signal. *Nature*. 395:645–648.
50. Negulescu, P.A., N. Shastri, and M.D. Cahalan. 1994. Intracellular calcium dependence of gene expression in single T lymphocytes. *Proc. Natl. Acad. Sci. USA*. 91:2873–2877.
51. Heissmeyer, V., F. Macian, S.H. Im, R. Varma, S. Feske, K. Venuprasad, H. Gu, Y.C. Liu, M.L. Dustin, and A. Rao. 2004. Calcineurin imposes T cell unresponsiveness through targeted proteolysis of signaling proteins. *Nat. Immunol.* 5:255–265.
52. Yamaguchi, T., D.P. Wallace, B.S. Magenheimer, S.J. Hempson, J.J. Grantham, and J.P. Calvet. 2004. Calcium restriction allows cAMP activation of the B-Raf/ERK pathway, switching cells to a cAMP-dependent growth-stimulated phenotype. *J. Biol. Chem.* 279: 40419–40430.
53. Dong, C., R.J. Davis, and R.A. Flavell. 2002. MAP kinases in the immune response. *Annu. Rev. Immunol.* 20:55–72.
54. Wu, C.C., S.C. Hsu, H.M. Shih, and M.Z. Lai. 2003. Nuclear factor of activated T cells c is a target of p38 mitogen-activated protein kinase in T cells. *Mol. Cell. Biol.* 23:6442–6454.
55. Avots, A., M. Buttmann, S. Chuvpilo, C. Escher, U. Smola, A.J. Bannister, U.R. Rapp, T. Kouzarides, and E. Serfling. 1999. CBP/p300 integrates Raf/Rac-signaling pathways in the transcriptional induction of NF-ATc during T cell activation. *Immunity*. 10: 515–524.
56. Kupzig, S., S.A. Walker, and P.J. Cullen. 2005. The frequencies of calcium oscillations are optimized for efficient calcium-mediated activation of Ras and the ERK/MAPK cascade. *Proc. Natl. Acad. Sci. USA*. 102:7577–7582.
57. Peng, S.L., A.J. Gerth, A.M. Ranger, and L.H. Glimcher. 2001. NFATc1 and NFATc2 together control both T and B cell activation and differentiation. *Immunity*. 14:13–20.
58. Rengarajan, J., B. Tang, and L.H. Glimcher. 2002. NFATc2 and NFATc3 regulate T_H2 differentiation and modulate TCR-responsiveness of naive T_H cells. *Nat. Immunol.* 3:48–54.